AIAA-2001-2462
Reynolds Number Effects on Leading Edge Radius Variations of a Supersonic Transport at Transonic Conditions

S. M. B. Rivers, R. A. Wahls, and L. R. Owens
NASA Langley Research Center
Hampton, Virginia

19th AIAA Applied Aerodynamics Conference
11-14 June 2001
Anaheim, California

REYNOLDS NUMBER EFFECTS ON LEADING EDGE RADIUS VARIATIONS OF A SUPERSONIC TRANSPORT AT TRANSONIC CONDITIONS

S. M. B. Rivers[*], R. A. Wahls[†], and L. R. Owens[‡]
Aerodynamics, Aerothermodynamics, and Acoustics Competency
NASA Langley Research Center
Hampton, Virginia

ABSTRACT

A computational study focused on leading-edge radius effects and associated Reynolds number sensitivity for a High Speed Civil Transport configuration at transonic conditions was conducted as part of NASA's High Speed Research Program. The primary purposes were to assess the capabilities of CFD to predict Reynolds number effects for a range of leading-edge radius distributions on a second-generation supersonic transport configuration, and to evaluate the potential performance benefits of each at the transonic cruise condition. Five leading-edge radius distributions are described, and the potential performance benefit including the Reynolds number sensitivity for each is presented. Computational results for two leading-edge radius distributions are compared with experimental results acquired in the National Transonic Facility over a broad Reynolds number range.

[*] Aerospace Engineer, Configuration Aerodynamics Branch, Member, AIAA

[†] Assistant Head, Configuration Aerodynamics Branch, Associate Fellow, AIAA

[‡] Aerospace Engineer, Subsonic Aerodynamics Branch, Senior Member, AIAA

INTRODUCTION

The present investigation was conducted in support of NASA's High Speed Research (HSR) Program, Phase II, which was conducted from 1993-1999 (ref. 1). The objective of this NASA sponsored, jointly executed program with US industry, was to develop critical high-risk airframe and propulsion technologies to enable industry development of an economically viable and environmentally acceptable second-generation high speed civil transport (HSCT). Aerodynamic performance was one of several broad airframe technology areas, and included tasks to address Configuration Aerodynamics for high-speed conditions and High-Lift Technology for take-off and landing. These elements encompassed not only the challenge of efficient supersonic cruise flight, but also the off-design challenges (ref. 2) of efficient transonic cruise and acceleration and high-performance, quiet take-off and landing.

A configuration known as the Reference H was provided by Boeing and used as the basis for study including derivative design early in the program. The Reference H configuration represented a Mach 2.4, 300 passenger aircraft with a 5000 nautical mile range, and was characterized by its cranked-delta wing planform with a highly swept, blunt leading-edge (LE) inboard panel and a moderately swept, sharp LE outboard panel. The design of the outboard panel LE was driven by supersonic cruise considerations. During the course of the program, a second reference configuration was defined as the basis for further technology development; this configuration was known as the Technology Concept Airplane (TCA) and was defined based on results and lessons learned to that point in the program. The TCA, though different from the Reference H,

American Institute of Aeronautics and Astronautics

maintained a cranked-delta wing planform with a highly swept, blunt LE inboard panel and a moderately swept, sharp LE outboard panel. Similar to the earlier configuration, it was clear that the viability of a future HSCT would be significantly enhanced through improved low speed high-lift performance either through quieter engines and/or higher aerodynamic efficiency.

Leading-edge geometry changes can enhance performance at the off-design subsonic and transonic conditions, particularly if the less swept, outboard portion of the wing is allowed to contribute. However, performance enhancement at the off-design conditions cannot be made to the point of significantly degrading the supersonic cruise performance. Can improved subsonic performance by modification of a supersonic LE be realized without adversely affecting supersonic performance? A previous study by Wilby (ref. 3) showed a reduced drag airfoil at supersonic speeds incorporating a relatively blunt LE. The Natural Flow Wing design philosophy as applied in the redesign of a supersonic transport configuration in the HSR program demonstrated the possibilities (ref. 4) for this class of vehicle. The key to success was an integrated design; that is, the LE geometry cannot be changed independent of overall geometry to achieve the best result.

In addition to performance enhancing technology development, ground-to-flight scaling was a focus in the HSR program. Ground-to-flight scaling remains one of many challenges facing today's designers of aerospace vehicles, with the goal being the preflight prediction of multiple key aerodynamic characteristics with sufficient accuracy to meet both performance guarantees and certification requirements. Specific challenges, experiences, and suggested approaches to ground-to-flight scaling have been documented extensively over the years for a variety of vehicle classes (refs. 5, 6 among many others). Reynolds number effects are foremost among many factors affecting successful ground-to-flight scaling (refs. 7 - 9). The Reynolds number is the primary aerodynamic scaling parameter used to relate sub-scale wind tunnel models to full-scale aircraft in flight. The challenge of Reynolds number scaling increases as the size of the full-scale aircraft increases due to the increasing Reynolds number increment between that
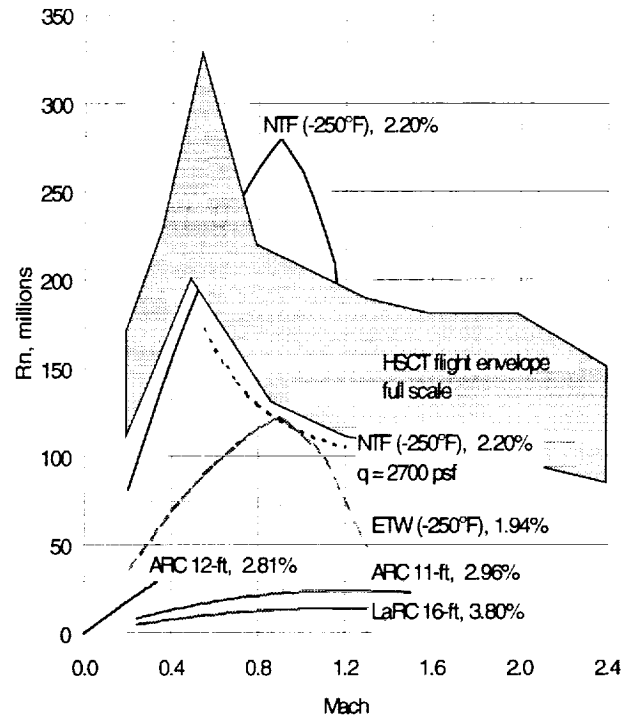

Figure 1. Nominal HSCT mission profile and wind tunnel capabilities (model scale adjusted to test section size).

obtainable in conventional wind tunnels and flight conditions. Figure 1 shows the nominal mission profile for the baseline reference configuration used in the HSR program and indicates the magnitude of the scaling issue for a vehicle the size of an HSCT.

The objective of the present study was to assess the capabilities of CFD to predict Reynolds number effects for a range of LE radius distributions on a second-generation supersonic transport configuration, and to evaluate the potential performance benefits of each at the transonic cruise condition. The use of CFD enabled an expanded study of LE geometry beyond that performed experimentally. The thin-layer Navier-Stokes flow solver CFL3D (ref. 10) was used with the Baldwin-Lomax (ref. 11) turbulence model, as modified by Degani-Schiff (ref. 12); this model was chosen after comparison with results using several other models. The CFD study included flow conditions at M=0.90, angles-of-attack ranging from 1 to 10 degrees and Reynolds numbers ranging from 11 to 88 million based on the mean aerodynamic chord. In this investigation, it is assumed that the boundary layer is turbulent everywhere.

TERMS, ABBREVIATIONS, & ACRONYMS

ARC   NASA Ames Research Center
c   local chord, in.
C_D drag coefficient
C_{DV} viscous drag coefficient
C_L lift coefficient
C_m pitching moment coefficient, referenced to 50% mean aerodynamic chord
ETW   European Transonic Windtunnel
HSCT   High Speed Civil Transport
HSR   High Speed Research
L/D   lift-to-drag ratio
LaRC   Langley Research Center
LE   leading edge
M   free-stream Mach number
NTF   National Transonic Facility
q   dynamic pressure, psf
r   radius, in.
Rn   Reynolds number based on mean aerodynamic chord
TCA   Technology Concept Airplane
x,y   Cartesian coordinates, in.
y^+ law-of-the-wall coordinate
α angle of attack, deg
η nondimensional semispan station

Figure 2. External view of the NTF.

Figure 3. NTF circuit diagram (linear dimensions in ft).

EXPERIMENTAL APPROACH

Facility Description

The NTF (ref. 13) is a unique national facility (Figure 2) that enables tests of aircraft configurations at conditions ranging from subsonic to low supersonic speeds at Reynolds numbers up to full-scale flight values, depending on the aircraft type and size. The facility (Figure 3) is a fan-driven, closed-circuit, continuous-flow, pressurized wind tunnel capable of operating in either dry air at warm temperatures or nitrogen from warm to cryogenic temperatures.

The test section is 8.2 ft by 8.2 ft in cross section and 25 ft in length. The test section floor and ceiling are slotted (6 percent open), and the sidewalls are solid. Free-stream turbulence is damped by four screens and a 14.95:1 contraction ratio from the settling chamber to the test section. Fan-noise effects are minimized by an acoustic treatment both upstream and downstream of the fan. A detailed assessment of the dynamic flow quality in the NTF is reported in reference 14, and reconfirmed with more recent measurements shown in reference 15. The NTF is capable of an absolute pressur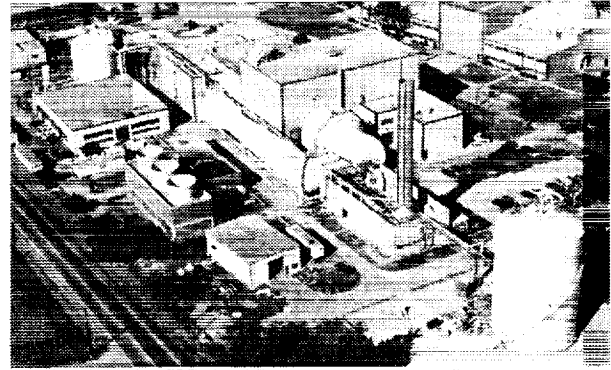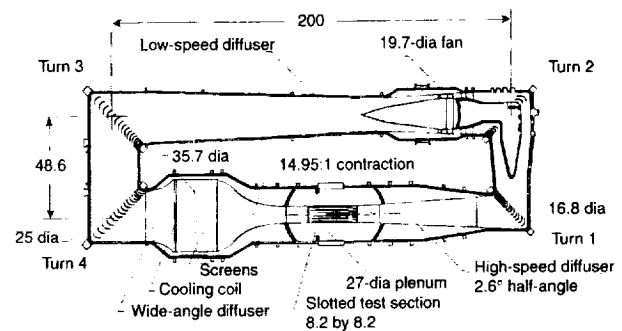e range from 15 psi to 125 psi, a temperature range from $-320°F$ to $150°F$, a Mach number range from 0.2 to 1.2, and a maximum Reynolds number of 146×10^6 per ft at Mach 1. Typical tests use temperatures ranging from -250 to $120°F$. Further facility details can be found in reference 16.

Model Description

The wind-tunnel model was a 2.2% scale modified representation of the initial HSR baseline configuration, and was known as the Modified Reference H configuration. The Modified Reference H model originated as a low-cost approach towards the evaluation of Reynolds number effects on a configuration with the planform and LE geometry of the HSR TCA configuration. The baseline Reference H model, described in references 17 and 18, was modified to provide the planform and LE radius distribution of the TCA. Figure 4 shows a comparison between the Reference H and Modified Reference H (TCA) wing planforms. Transition areas between the existing Reference H wing center section and the new, TCA-representative parts required localized blending. Outboard of $\eta=0.61$ (y=10.57 inches), both the airfoil shape and twist of the Modified Reference H model were identical to the TCA wing

3

definition. Inboard, however, the twist distribution and airfoil shape downstream of approximately 20 to 30% of the local chord were constrained to that of the existing Reference H wing center section. The resulting model geometry was smooth and sufficient to address the objectives of the required studies. However, in no way should this geometry be considered aerodynamically optimized.

The Modified Reference H model has a cranked-delta wing planform with an aspect ratio of 2.027, a span of 34.65 inches, a reference area of 4.114 ft^2, and a mean aerodynamic chord of 25.067 inches; pitching-moment data was referenced to the 50% mean aerodynamic chord location (x = 46.184 inches, figure 4). The inboard wing ($\eta \leq 0.61$) has a blunt, subsonic LE with a LE sweep of 71 degrees. The outboard, supersonic LE is swept 52 degrees. Interchangeable LE, TE, and outboard wing panel parts allow testing of two LE radius distributions, and configurations with flaps deflected for low speed, high lift assessment. Details of the baseline LE radius distribution and the one alternate distribution tested are provided below when describing the full suite of LE radius variations studied computationally herein.

Figure 4. Planform comparisons for the 2.2% scale model.
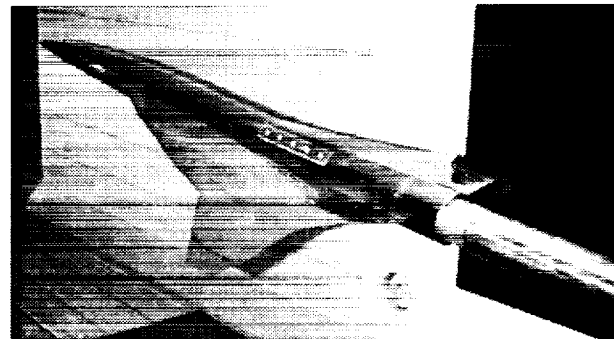
Figure 5. 2.2% Modified Reference H model in the NTF.

Wind Tunnel Test

The wind-tunnel model is shown in Figure 5 mounted in the NTF test section on a straight sting. Force and moment data used herein were acquired at Mach 0.90 over an angle-of-attack range from -2 to 12 deg for Reynolds numbers of 11, 33, and 88 million, based on the mean aerodynamic chord. Dynamic pressure was varied from approximately 970 to 1800 psf, and included a dynamic pressure sweep at Rn=33 million to isolate and enable correction for static aeroelastic effects as described in reference 18. Detailed information on the various instrumentation devices, the data acquisition and control computers, and the data reduction algorithms is provided in reference 19, including corrections for free-stream flow angularity and cavity pressure effects. Wall and model support interference effects have not been accounted for in the data, but were minimized through model sizing (ref. 18). All data presented herein was acquired with fixed transition on the forebody, as described in reference 18, and natural transition on the wing. Data repeatability was determined as described in reference 18, and can be characterized with 95% confidence intervals of
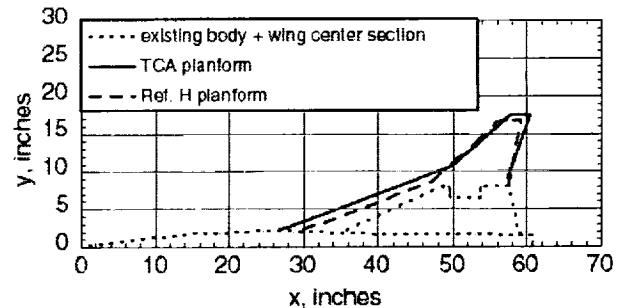
±0.0015, ±0.0002, and ±0.0002 for lift, drag, and pitching-moment coefficients, respectively.

COMPUTATIONAL APPROACH

Computational Algorithm

The computational method used in this study was version 4.1 of the Navier-Stokes flow solver known as CFL3D. The code solves the 3-D time-dependent thin-layer Navier-Stokes equations with a finite-volume formulation. The governing equations are discretized to be consistent with conservation laws in integral form, and are solved using a second-order accurate upwind-biased spatial differencing scheme. Roe's flux-difference splitting (ref. 20) is used to construct the upwind differences for the convective and the pressure terms. The spatial derivatives are written conservatively as a flux balance across the cell, and the shear stress and heat transfer terms are centrally differenced. Spatial approximate factorization and Euler backward integration after linearization in time results in the solution through 5x5 block-tridiagonal matrix inversions in three directions. An approximate diagonal form of the spatial factors is employed to reduce

computational time. Convergence acceleration is obtained by using a multigrid full-approximation scheme and mesh sequencing for flow initialization. Reference 10 gives a complete description of this code.

Turbulence Model

The Reynolds stresses are modeled using one of four turbulence models implemented in the flow solver: Spalart-Allmaras, Baldwin-Lomax with the Degani Schiff modifications (B-L), Baldwin-Barth, and Menter's SST. A short turbulence model study was conducted to select a single model for use in the current investigation. Results of this study are shown in figure 6, and indicate that each model overpredicted the drag for each Reynolds number at the nominal cruise angle of attack. At this stage in the investigation, the B-L model produced the best comparison with the experimental results, and was selected for further use. Similar results were reported in a previous, more detailed turbulence model study on a similar configuration at similar conditions (ref. 21). Later in the investigation, when static aeroelastic corrections to the wind tunnel data became available, a different choice of model may have been made as this correction would shift the experimental data shown in figure 6 upward into the cluster of computational results.

The Baldwin-Lomax turbulence model (ref. 11) has been used widely within the CFD community over the years; its capabilities and limitations are well known. In short, it is generally considered a good model for the prediction of attached flows, but it is deficient for flows with any significant separated regions. In particular, the Baldwin-Lomax model tends to predict shocks too far downstream for separated transonic flows over aerodynamic configurations. Degani and Schiff (ref. 12) modified the original Baldwin-Lomax model to enable a more accurate determination of the viscous length scale for high-angle-of-attack flows in regions of cross flow separation, where a strong leeward vortical flow structure exists. As noted above, it is the Baldwin-Lomax turbulence model as modified by Degani and Schiff that is used herein. It is acknowledged that the Spalart-Allmaras model has become the turbulence model of choice for many CFD users today, and that it likely would have been chosen had this investigation been initiated today. Nevertheless, the B-L model provided sufficient, consistent results during the current investigation.
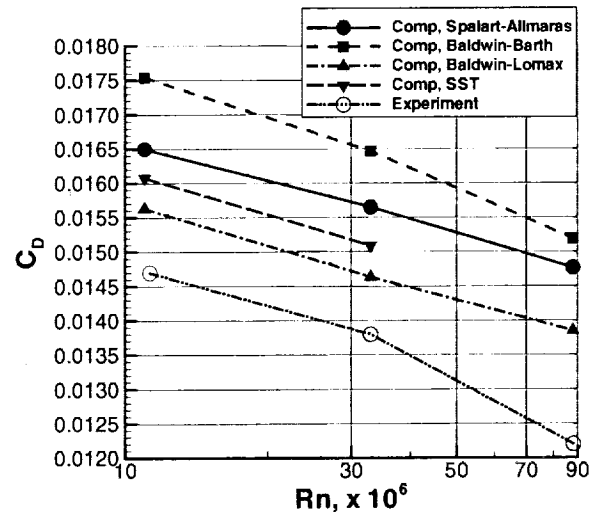

Figure 6. Reynolds number effects on predicted drag using various turbulence models, M=0.9, α=5.0 deg, baseline Modified Reference H.

Surface Geometry and Grid Generation

Five surface grids were generated to model the baseline Modified Reference H configuration and four alternate configurations characterized by different LE radius distributions. Throughout this paper, the five configurations are designated as follows: 1) baseline LE, 2) full blunt LE, 3) full sharp LE, 4) blunt to sharp LE, and 5) sharp to blunt LE. Figures 7 and 8 specifically define each LE radius distribution. The baseline is that of the baseline Modified Reference H configuration and is identical to that of the TCA configuration. The baseline distribution is characterized by a blunt inboard LE with an abrupt change to a sharp LE outboard as highlighted in Figure 9. Each alternate configuration incorporated a systematic variation of the LE radius about the baseline.

The full blunt LE matches the inboard LE of the baseline, then maintains the blunt r/c ratio at the planform break across the entire outboard panel. The surface grid in the region of the planform break is shown in Figure 10. In addition to the baseline, computational results for this configuration are compared with experimental results.

The full sharp LE is identical to the baseline on the outboard wing panel, in addition to being sharp (r=0) inboard. Figure 11 shows this grid in the region of the planform break. The blunt to sharp LE begins with the baseline radius at the side of body, decreases linearly to zero at the tip. This configuration provides a smooth

5

variation across the LE constrained to match the baseline at the side of body and wing tip; Figure 12 highlights this grid in the region of the planform break. Finally, the sharp to blunt LE begins with r=0 at the side of body, then linearly increases to that of the full blunt LE at the tip; Figure 13 highlights this grid in the region of the planform break. The full sharp, blunt to sharp, and sharp to blunt LE distributions were not tested experimentally.

A total of ten grids were generated and used herein to show the effect of Reynolds number on five different configurations. A typical volume grid is shown in Figure 14. The volume grids for each configuration consisted of a single C-O grid topology (C in the stream wise direction and O in the span wise direction). The grids had 141 points in the stream wise direction, 257 points in the span wise direction and 65 points in the normal direction, totaling approximately 2.4 million grid points. The normal spacing adjacent to the surface was $5x10^{-5}$ inches over the entire surface for Rn=11 and 33 million, and $1x10^{-5}$ inches over the entire surface for Rn=88 million. These surface spacing distributions provide nondimensional y^+ values of approximately one for each Reynolds number at Mach 0.90.
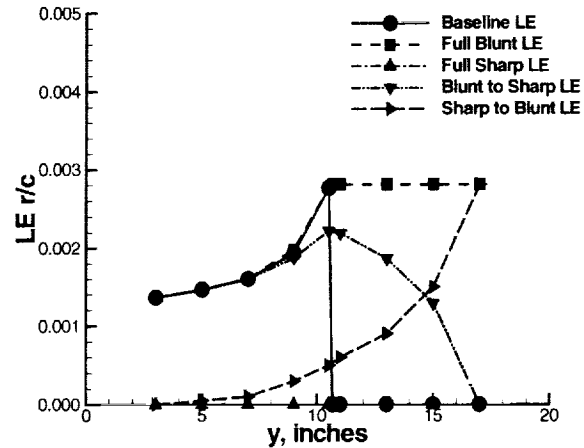
Figure 8. Dimensionless baseline and alternate LE radius distributions.
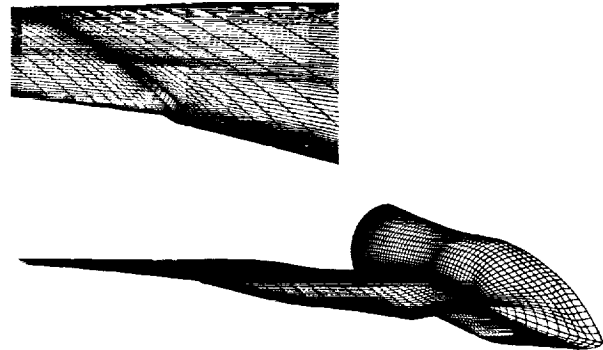
Figure 9. Modified Reference H baseline configuration.
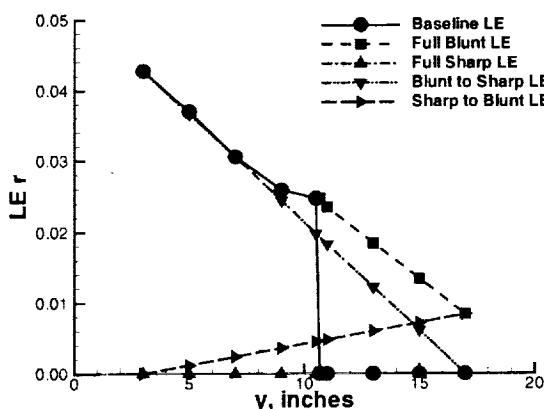
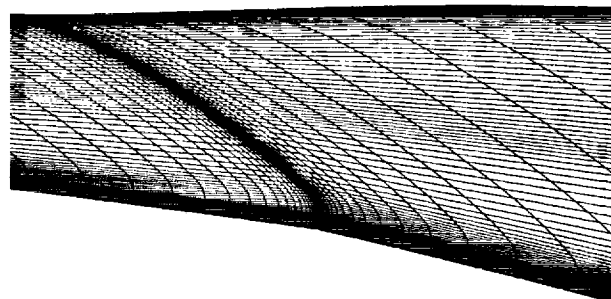Figure 7. Baseline and alternate LE radius distributions, Modified Reference H.

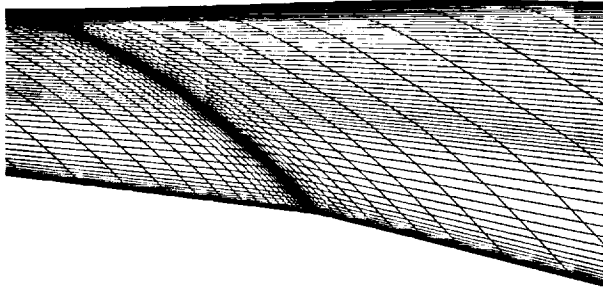Figure 10. Modified Reference H configuration with the full blunt LE.

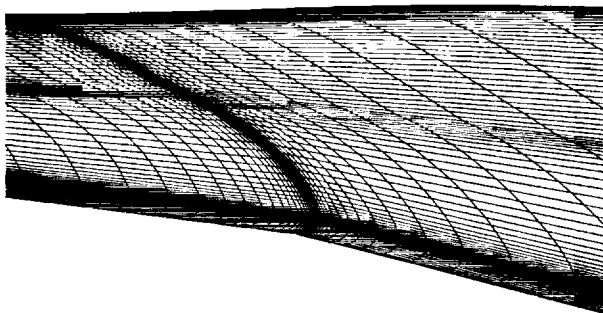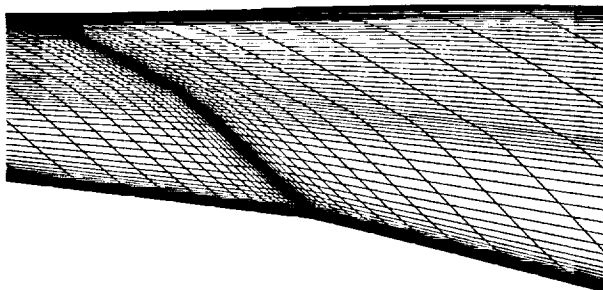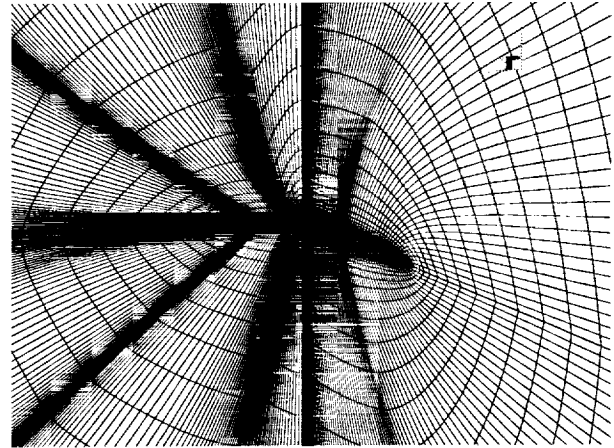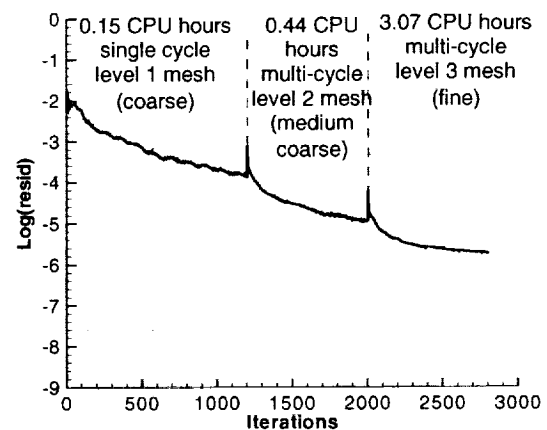Figure 11. Modified Reference H configuration with a full sharp LE.

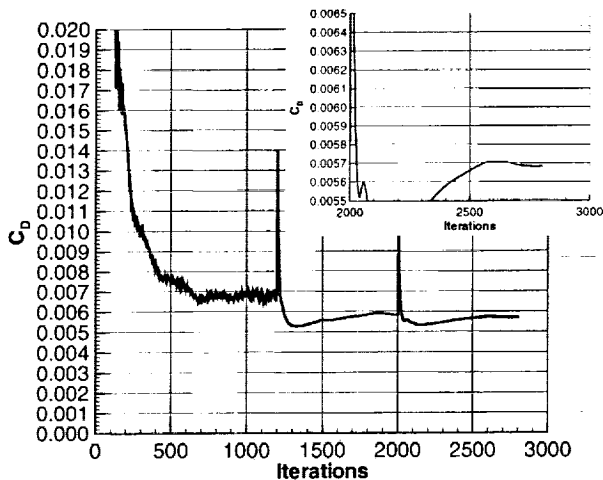Figure 14. Modified Reference H volume grid.

Convergence

The solutions for this study were considered converged when the drag coefficient changed less than one count (0.0001) over 100 iterations and the residual decreased by at least three orders of magnitude. A typical convergence history is shown in Figure 15. This figure shows the convergence history for the $\alpha=1$ deg case at Rn=33 million on the full blunt LE configuration. The run procedure along with the computational time is given. First, the flow is initialized on two coarser grids, and then the solution is interpolated onto the finest mesh where iterations are performed until convergence is reached. The full sharp LE configuration did not converge at Rn=88 million, therefore no results will be shown for this case. All computations were made on the Langley Cray YMP and the NAS Cray C-90. All computation times given in the figure are in C-90 equivalent CPU hours.

Figure 12. Modified Reference H configuration with a blunt to sharp LE.

Figure 13. Modified Reference H configuration with a sharp to blunt LE.

a)   Residual history

Figure 15. Typical convergence history $\alpha=1.0$ deg case, Rn=33x10^6, full blunt LE.

American Institute of Aeronautics and Astronautics

b) Drag history

Figure 15. Concluded.

RESULTS AND DISCUSSION

The primary purposes of this investigation were to assess the capabilities of CFD to predict Reynolds number effects for a range of LE radius distributions on a realistic HSCT configuration and to evaluate the potential performance benefits of each radius distribution at the transonic cruise condition. First, computational results for two LE radius distributions are compared with experimental results acquired in the NTF over a broad Reynolds number range. Then, computational results for all LE radius distributions are compared to assess the relative performance benefit of each.
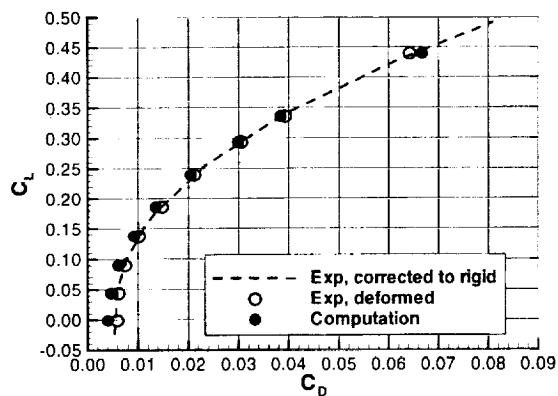
Computation to Experiment Comparisons

Figures 16 and 17 provide longitudinal force and moment coefficient comparisons between computation and experiment for the baseline and full blunt LE radius distributions, respectively. The data shown is for Rn = 88 million, the highest Reynolds number studied; comparisons at low and moderate Reynolds numbers (11 and 33 million) are similar. All experimental data has been corrected for static aeroelastic deformation effects to the rigid, wind-off shape as used in the computations. The corrections were made in a manner similar to that described in reference 18, with the aeroelastic sensitivities determined in the wind tunnel using the specialized capabilities of the NTF for such purposes. Experimental data points shown are limited to those near the

nominal angles-of-attack used in the computations; the drag-coefficient data shown was determined by interpolation to consistent, nominal lift coefficients to facilitate the comparisons.

Comparisons for the baseline configuration, figure 16, indicate an offset for drag, and generally good agreement for lift and pitching moment. The drag data shows that the computations predict lower values than determined in the experiment, and it is clear even on the coarse scale shown. The effect is highlighted in terms of lift-to-drag ratio, particularly near maximum L/D. However, the general character of L/D, including the lift coefficient for maximum L/D is predicted well. Lift and pitching moment comparisons highlight the importance of corrections for static aeroelastic effects. Lift comparisons are excellent up to approximately 6-7 deg, at which point separation is beginning to dominate the flow field. The pitching moment comparison is generally good also, though there is a small shift in the zero-lift characteristics. For reference, a pitching-moment change of approximately 0.005 is roughly equivalent to a one-degree change in the stabilizer angle for a full configuration with empennage in this vehicle class.

Comparisons for the full blunt LE configuration, figure 17, are generally the same as for the baseline configuration. The under prediction of the computation for each configuration ranges from approximately 5 to 15 drag counts in the predominately attached flow regime; this result reverses (i.e. the computation over predicts drag by approximately 15 counts) when the flow is predominately separated. This general result holds for the low and moderate Reynolds number data not shown in these figures. Examples of computation to experiment comparisons as a function of Reynolds number will be shown at selected angles of attack in the following section.
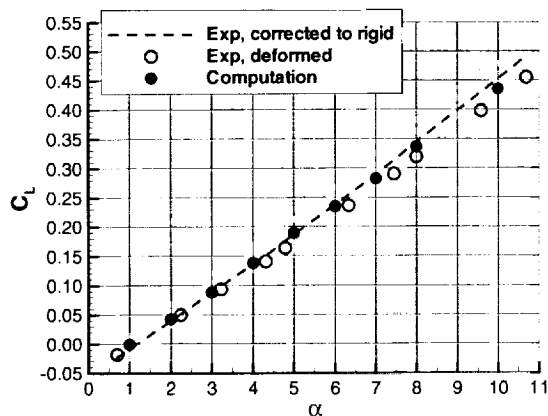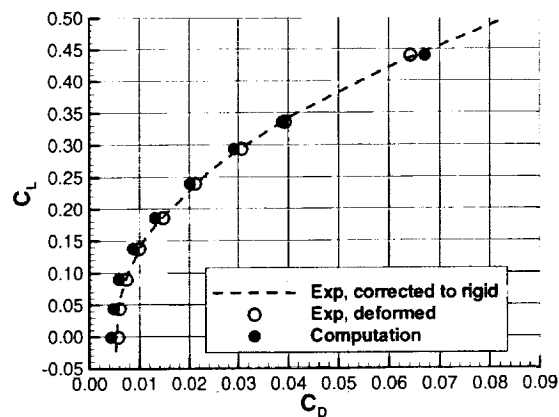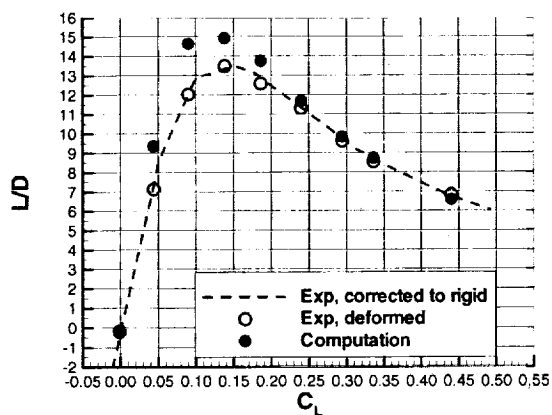
8
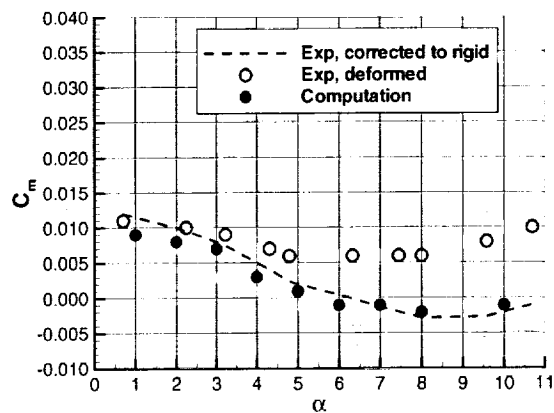
a) Drag polar

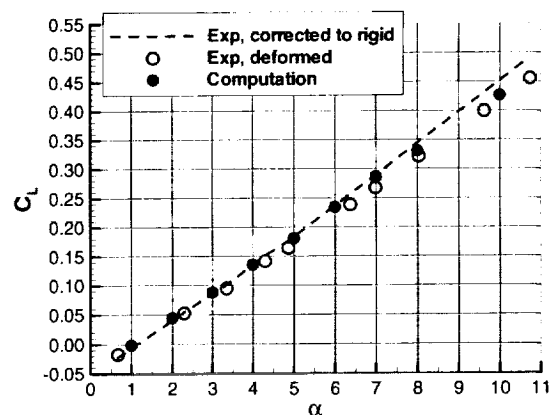d) Pitching Moment Curve
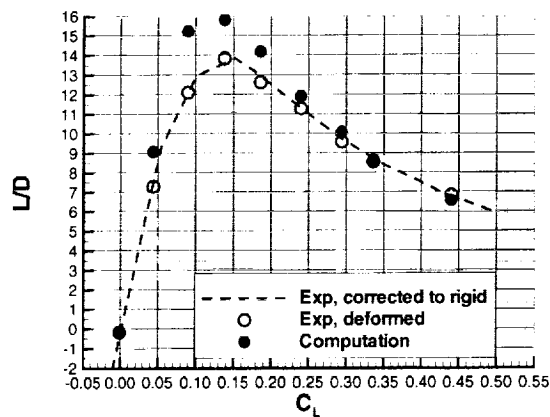
Figure 16. Concluded.

b) Lift curve

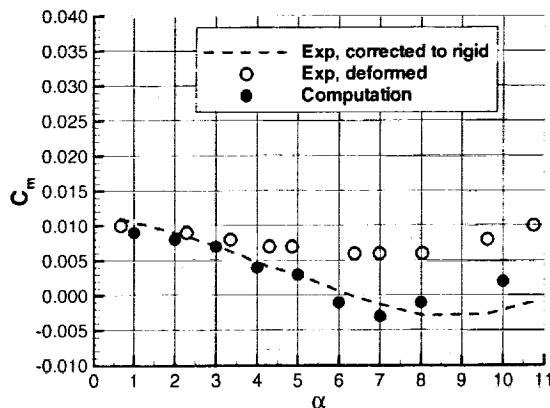a) Drag polar

c) Lift-to-Drag Ratio

Figure 16. Force and moment coefficients, baseline LE, M=0.90, Rn=88x10⁶.

b) Lift curve

Figure 17. Force and moment coefficients, full blunt LE, M=0.90, Rn=88x10⁶.

c)   Lift-to-Drag Ratio

d)   Pitching Moment Curve

Figure 17. Concluded.

LE Performance Comparisons

Figures 18 – 20 provide longitudinal force and moment coefficient comparisons for the baseline and four alternate LE radius distribution configurations as a function of Reynolds number for three angles of attack, as follows: 1) near minimum drag (α=1 deg), 2) near transonic cruise (α=5 deg), and 3) high angle of attack with significant wing leading-edge separation (α=10 deg), respectively. Experimental data, corrected for static aeroelastic effects, is provided for comparison as well. Each figure presents data in both absolute terms (on the left) and as increments determined as differences from the baseline configuration (on the right). Computational increments are based on the baseline from computation, and experimental increments are based on the baseline from experiment.

The near minimum drag condition is presented in Figure 18. This condition is clearly off-design for transonic cruise, but serves as a reference point for fully attached flow. As one would expect, drag decreases as a function of Reynolds number and is mostly accounted for by the established trend of skin friction with Reynolds number. It is also seen that the experimental drag is consistently higher than the computed drag. Figure 21 compares theoretical skin friction drag based on equivalent flat plate theory with form factors to the viscous drag component of the total drag from the computations; theory in this figure assumes fully turbulent flow. The fact that the computational viscous drag is 10 to 15 counts below theory may indicate that the viscous drag computation is the primary cause for the under prediction of drag relative to experimental data mentioned previously. As shown in Figure 18, the Reynolds number sensitivity of drag is similar for all LE's, and there is not a significant benefit or penalty associated with any alternate LE relative to the baseline. The computational drag values are more sensitive to Rn changes than the experimentally measured drag on both the baseline and full blunt LE configurations. Lift at this condition is insensitive to Reynolds number for all configurations, and no LE distinguishes itself as significantly different from the others.

The lift-to-drag ratio shows no significant difference between LE's and both the experimental data and computational data are Rn insensitive. Likewise, the pitching moment

data show no significant difference between LE's and each is essentially Rn insensitive.

Figure 19 presents results near the nominal transonic cruise condition; this is a condition at which the aircraft would fly a significant portion of its mission. As at the near minimum drag condition, the drag associated with each LE decreases with increasing Rn in a manner consistent with skin friction drag reduction. However, there is significant variation in the drag level between LE's at each Rn for the nominal cruise condition. Relative to the baseline, the full sharp and sharp to blunt LE's cause a drag increase on the order of 10 counts. The blunt to sharp and full blunt LE's generally provide drag decrease from 1 to 10 counts, depending on the LE and Rn. The drag changes relative to the baseline are not highly Rn sensitive, but do show some small decrease in benefit at the highest Rn condition. The lift coefficient is relatively insensitive to Rn; the general trend relative to the baseline is a lift reduction with increasing Rn for each LE. The lift-to-drag ratio, like the drag coefficient, is very sensitive to Rn for each LE; again, this is mostly due to skin friction changes at this angle of attack. The blunt to sharp LE provides the largest increase in L/D (~1 at Rn = 33 million) relative to the baseline, but the benefit is non-monotonic and drops significantly at Rn of 88 million. The full blunt LE, however, provides essentially the same L/D increase at 88 million. The sharp to blunt and full sharp LE's provide a nearly constant L/D reduction of approximately 1 across the Rn range. The pitching moment is relatively insensitive to Rn for each LE, as are the increments relative to the baseline. The configurations with relatively sharper inboard LE radius distributions provide the most nose-up moment relative to the baseline LE. The more nose up moment for the sharper inboard LE's suggests that blunting the inboard LE radius is necessary to delay the inboard LE flow separation ahead of the moment reference center. The configurations with both blunt inboard LE's and blunter outboard LE's also provide a small amount of nose-up moment relative to the baseline LE. The delay of the outboard LE separation reduces the vortex lift behind the moment reference center, which produces a small nose up moment relative to the baseline LE. The reduction of vortex lift on the outboard wing for the blunter outboard LE's also explains the drag reduction observed for these LE's relative to the baseline LE.

Figure 20 presents results at an off-design, high angle-of-attack condition with predominantly separated flow. As at the lower angles of attack, the drag decreases with increasing Rn up to 33 million, but no further drag reduction occurs at Rn of 88 million. Both the computational and experimental drag trends with Rn are similar. The full sharp and sharp to blunt LE's produce drag increases on the order of 30-40 counts, while the blunt to sharp and full blunt LE's provide much less change; in all cases, drag changes relative to the baseline are non-monotonic. The lift coefficient is relatively insensitive to Rn; most of the LE's provide slightly less lift relative to the baseline LE. The lift-to-drag ratio at this off-design condition is relatively insensitive to Rn; again the LE distributions with a sharper inboard LE radius consistently show a lower L/D relative to the baseline LE. The other LE's show no benefit over the baseline LE at this off-design condition. The pitching moment trend with Rn is similar to that observed for drag at this condition. The pitching moment changes relative to the baseline LE suggest that the LE configurations with a sharper inboard LE radius have more nose up moment than the other LE's. The reasons for the relative moment performance of each LE are the same as those discussed for the transonic cruise condition at $\alpha=5$ deg.
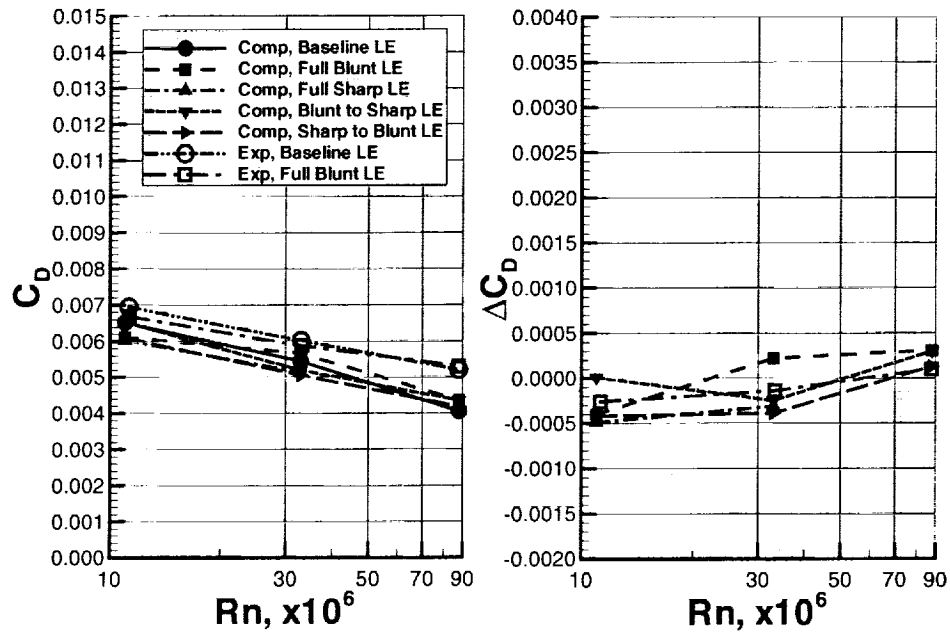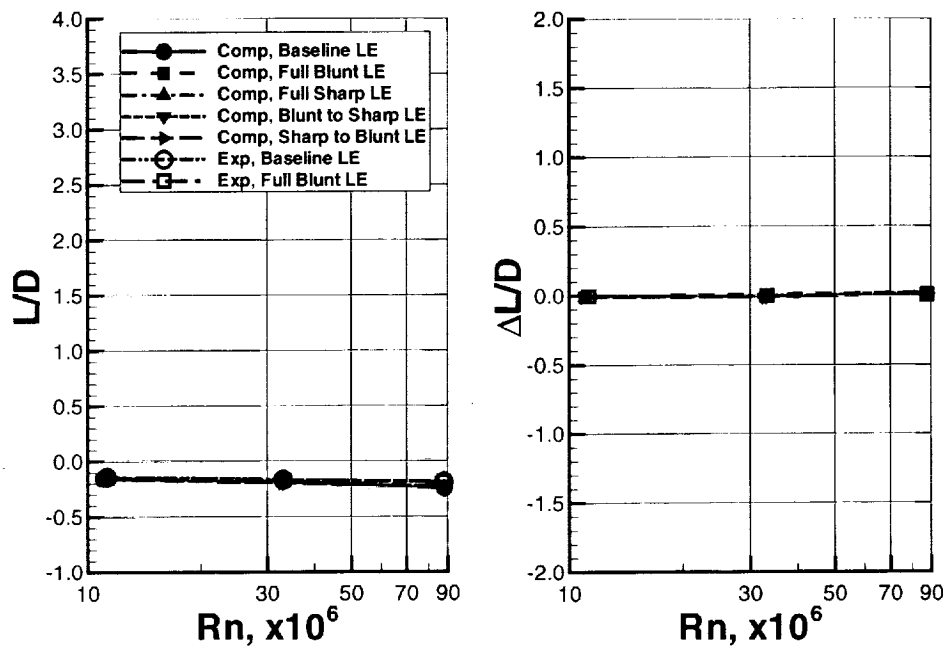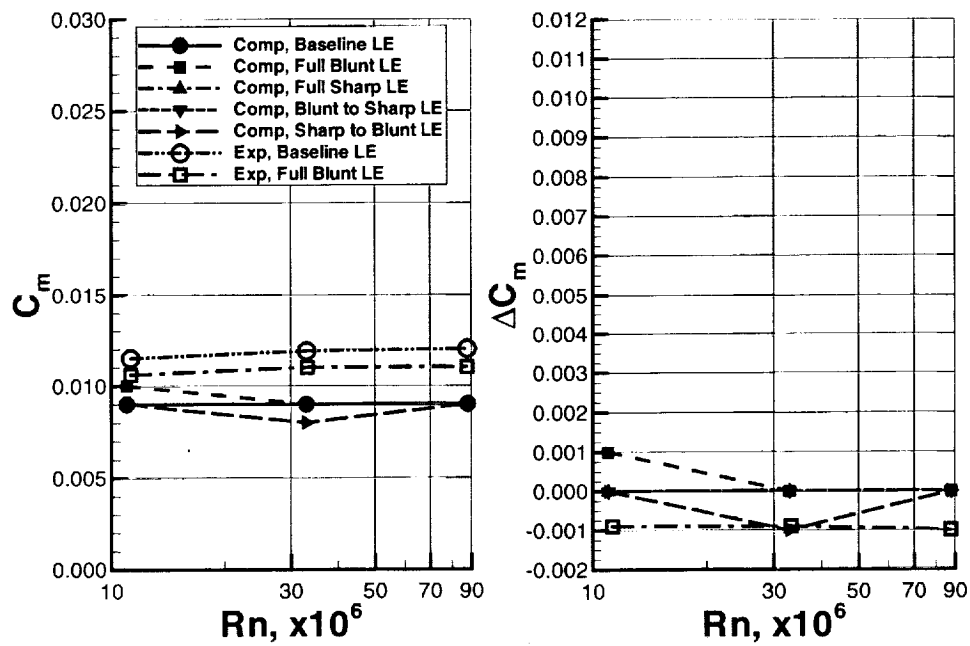
a)   Drag Coefficient
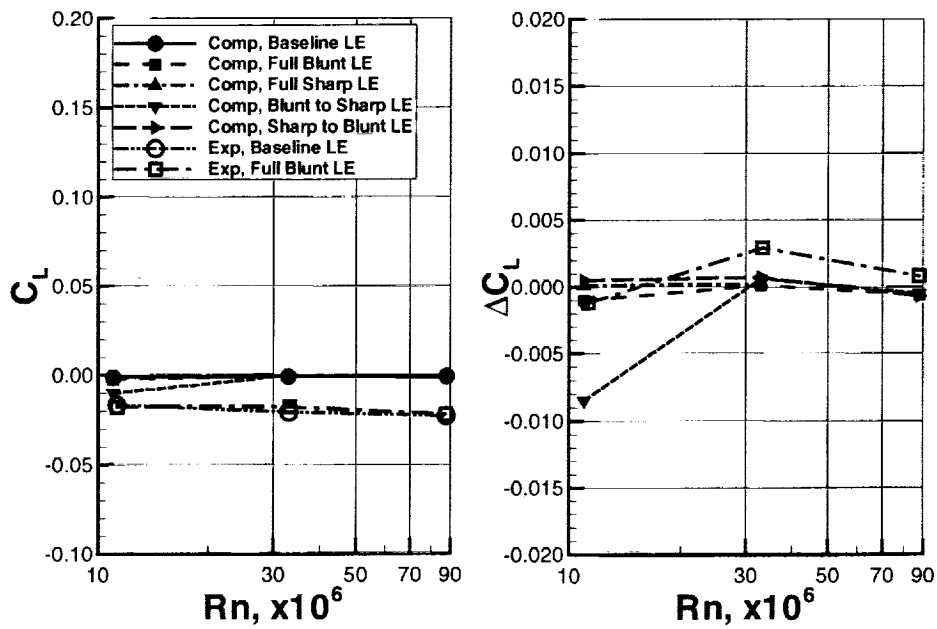
b)   Lift Coefficient

Figure 18. Longitudinal coefficient trends with Reynolds number, near minimum drag (α=1.0), M=0.90. (Delta values are referenced to the baseline LE values).
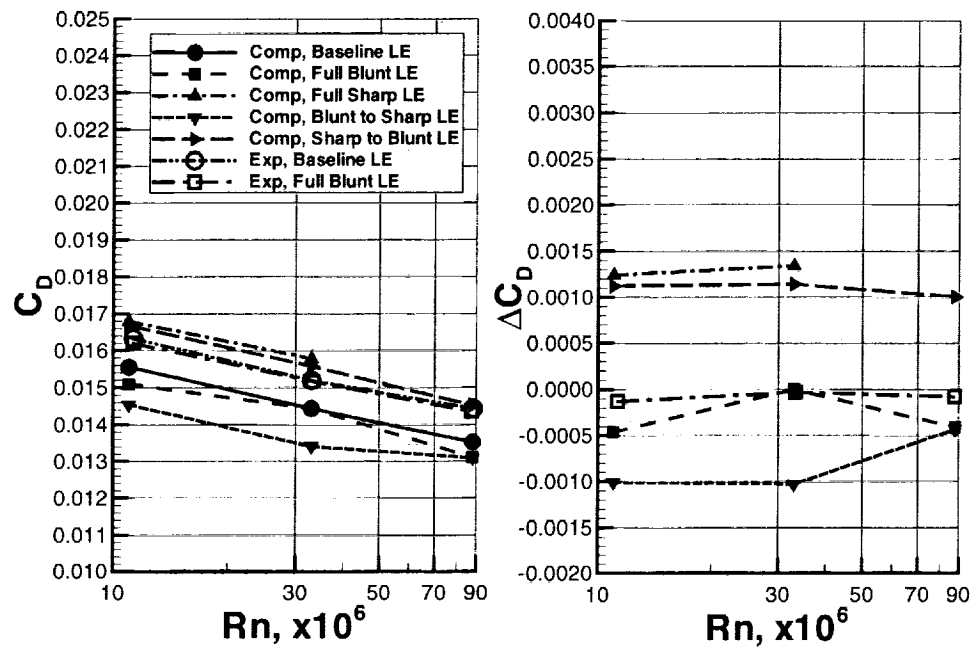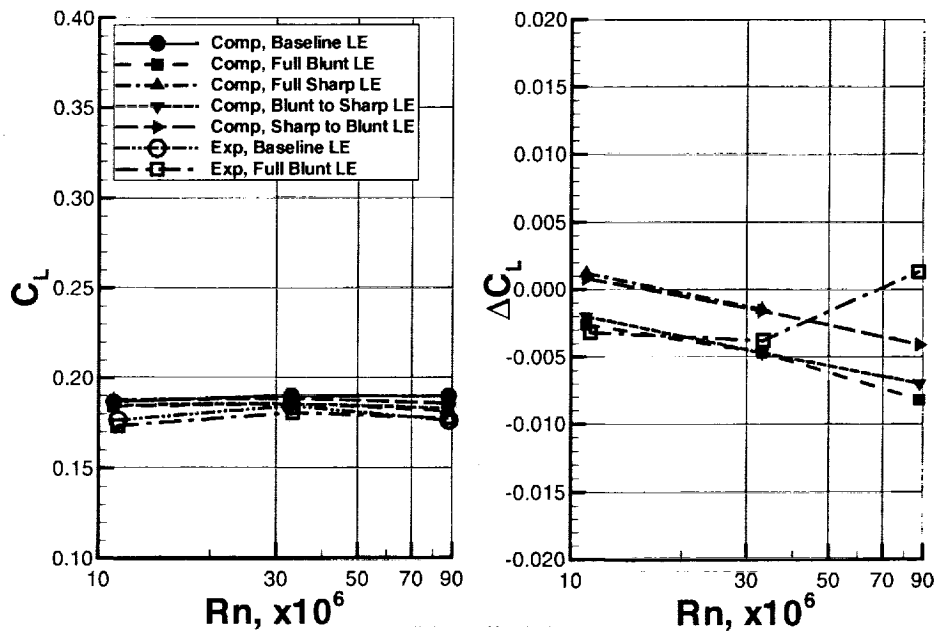
c)   Lift-to-Drag Ratio
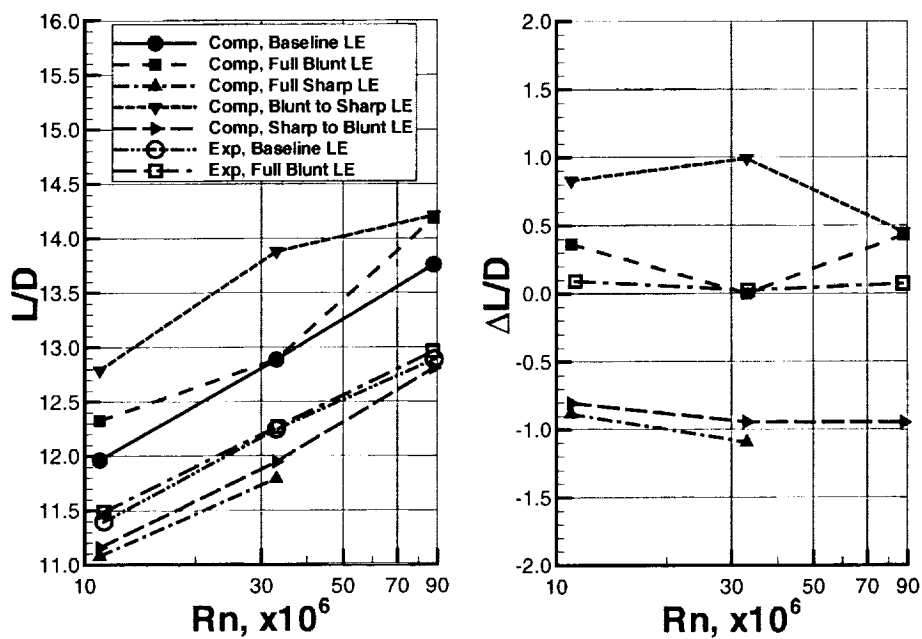
d)   Pitching Moment
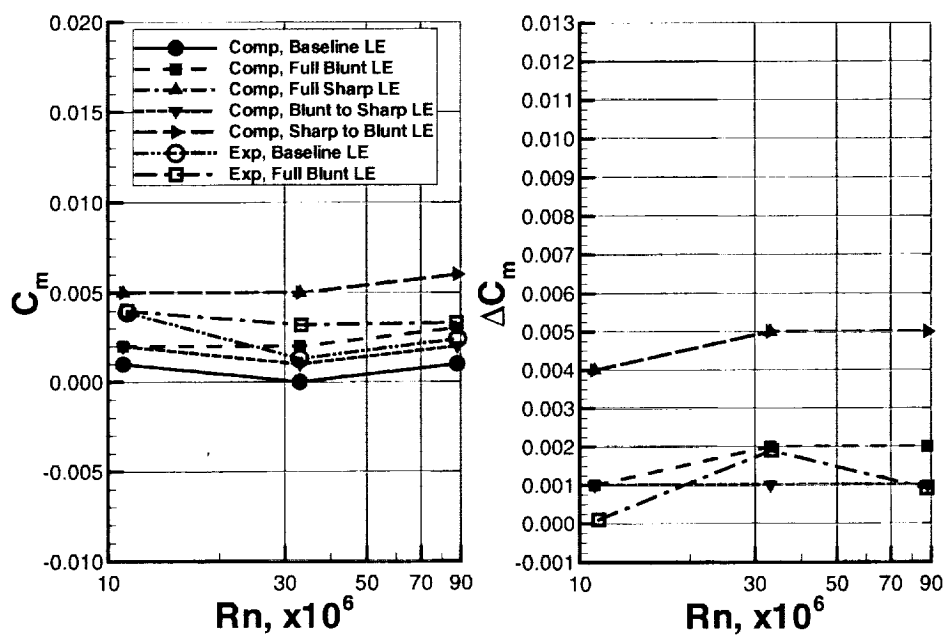
Figure 18. Concluded.

13

a)   Drag Coefficient

b)   Lift Coefficient

Figure 19. Longitudinal coefficient trends with Reynolds number, near transonic cruise (α=5.0), M=0.90. (Delta values are referenced to the baseline LE values).
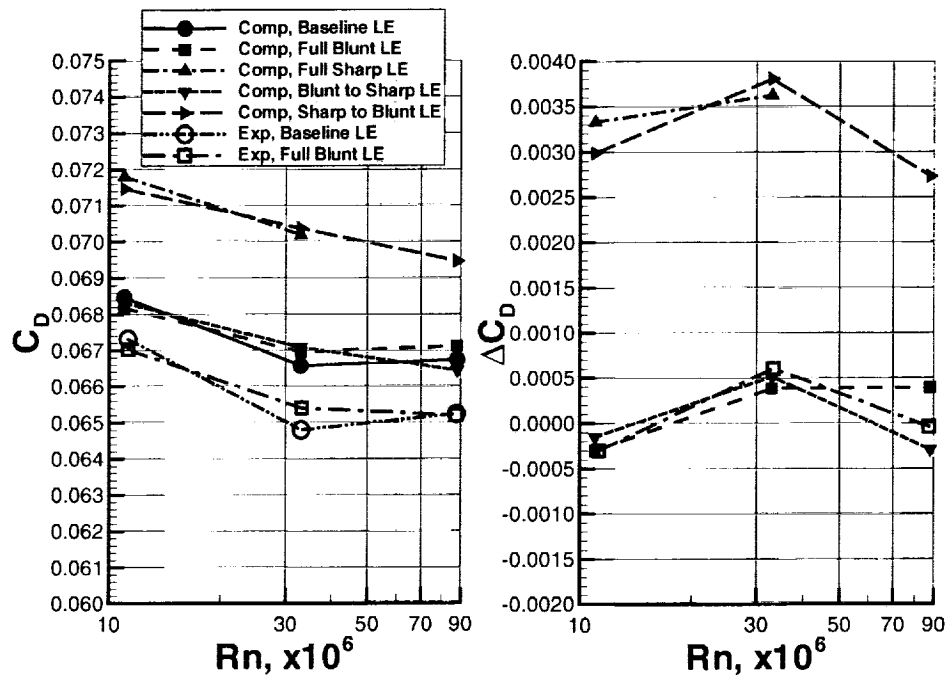
14

American Institute of Aeronautics and Astronautics

c)   Lift-to-Drag Ratio

d)   Pitching Moment

Figure 19. Concluded

American Institute of Aeronautics and Astronautics
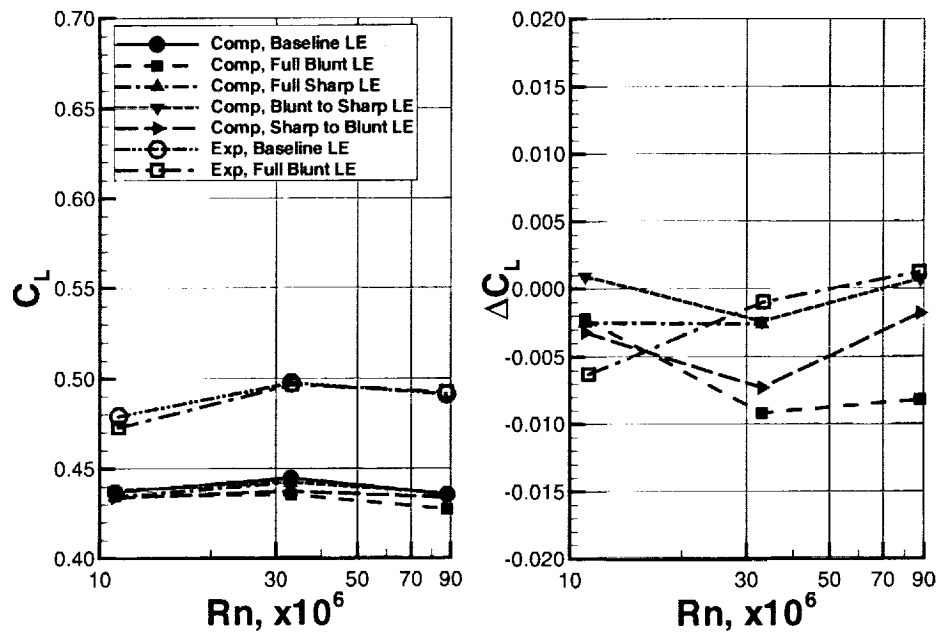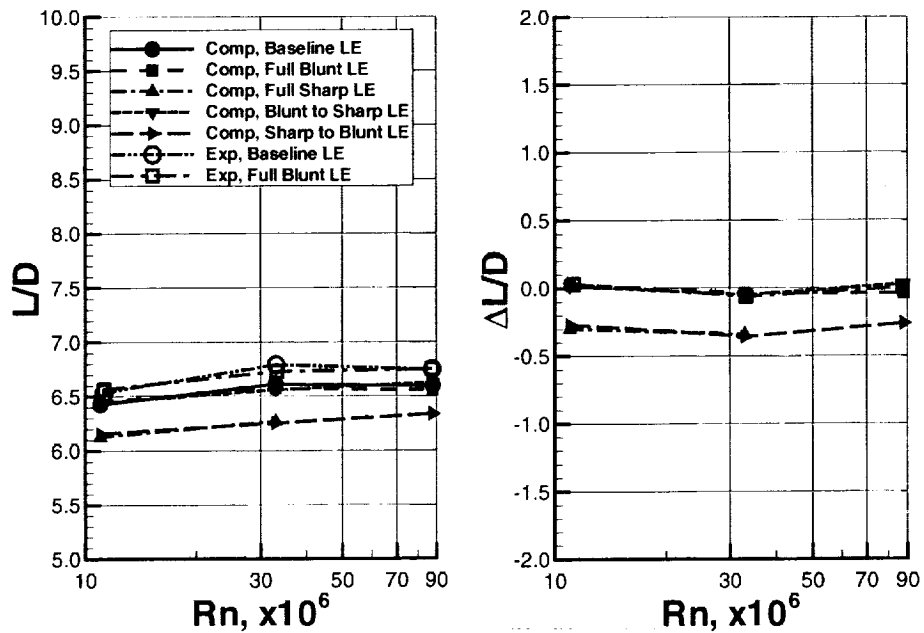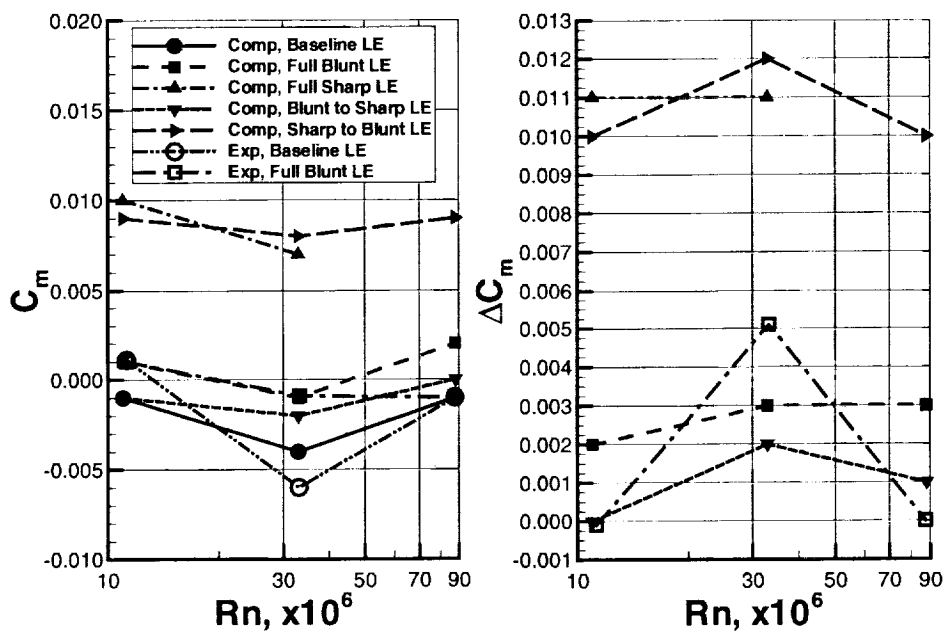
a)   Drag Coefficient

b)   Lift Coefficient

Figure 20. Longitudinal coefficient trends with Reynolds number, high angle of attack (α=10.0), M=0.90. (Delta values are referenced to the baseline LE values).

American Institute of Aeronautics and Astronautics

c) Lift-to-Drag Ratio

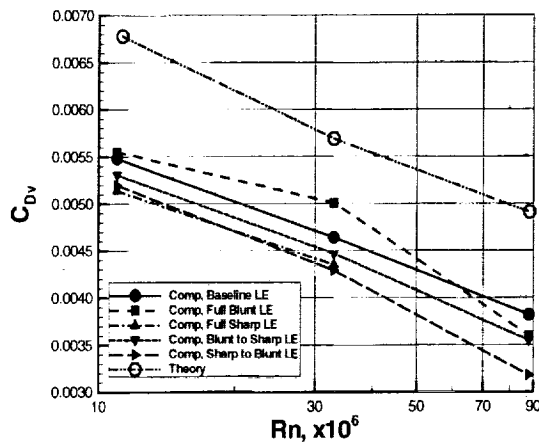d) Pitching Moment

Figure 20. Concluded.

17

Figure 21. Reynolds number effects on viscous drag.

CONCLUDING REMARKS

A computational study using a thin-layer Navier-Stokes flow solver was executed to complement and expand an experimental assessment of performance benefits and Rn sensitivities associated with various LE radius distributions on a relevant HSCT configuration. A baseline and four alternate LE radius distributions were described and evaluated at the transonic cruise Mach number of 0.90. Results were presented comparing computational predictions with experimental results obtained for two LE configurations in the NTF over a broad Rn range. Additionally, computational results for all five LE radius distributions were compared to assess the relative performance benefit of each, and their sensitivity to Rn changes. General conclusions are summarized as follows:

1. Corrections for static aeroelastic effects are important when one desires a direct comparison of computation to experiment, particularly for lift and pitching-moment characteristics.

2. Predictions of lift and pitching-moment characteristics were generally good. Drag, and thus L/D, predictions were generally offset from experimental results, though trends with angle of attack and Reynolds number were predicted reasonably well. It is believed most of the offset in drag is due to viscous drag prediction.

3. At the nominal cruise angle of attack, the blunter LE's provided more favorable performance increments. Continuity of the LE radius distribution across the LE planform break is an important factor in improved performance relative to the baseline as well. At off-design α's,

performance was less affected by LE radius variations.

4. Performance benefits of various LE radius distributions are not highly Rn sensitive, though some of the benefits relative to the baseline LE appeared to decrease at the highest Rn conditions.

REFERENCES

1. Wilhite, A. W., and Shaw, R. J.: "An Overview of NASA's High-Speed Research Program," 20th ICAS Congress, Paper 112, August 2000.

2. Nelson, C.P.: "Effects of Wing Planform on HSCT Off-Design Aerodynamics," AIAA Paper 92-2629, June 1992.

3. Wilby , P.G.: "The Pressure Drag of an Aerofoil with Six Different Round Leading Edges, at Transonic and Low Supersonic Speeds," ARC CP-921, January, 1966.

4. Bauer, S. X. S. and Krist, S.E.: "The Application of the NFW Design Philosophy to the HSR Arrow Wing Configuration," First NASA/Industry High Speed Research Configuration Aerodynamics Workshop, December 1999, NASA CP-1999-209690, Vol. 2, p. 597-639.

5. McKinney, L.W. and Baals, D.D. (editors): "Wind-Tunnel/Flight Correlation – 1981," NASA CP 2225, November 1981.

6. "Boundary-Layer Simulation and Control in Wind Tunnels," AGARD AR-224, Report of the Fluid Dynamics Panel Working Group 09, 1988.

7. Goldhammer, M.E. and Steinle, F.W. Jr.: "Design and Validation of Advanced Transonic Wings Using CFD and Very High Reynolds Number Wind Tunnel Testing," 17th ICAS Congress, September 1990.

8. Lynch, F.T.: "Experimental Necessities for Subsonic Transport Configuration Development," AIAA Paper 92-0158, January 1992.

9. Bushnell, D.M., Yip, L.P., Yao, C.S., Lin, J.C., Lawing, P.L., Batina, J.T., Hardin, J.C., Horvath, T.J., Fenbert, J.W., and Domack, C.S.: "Reynolds Number Influences in Aeronautics," NASA TM 107730, May 1993.

10. Thomas, J., Krist, S., and Anderson, W.: "Navier-Stokes Computations of Vortical Flows Over Low-Aspect-Ratio Wings," AIAA Journal, Vol. 28, No. 2, pp. 205-212, 1990.

18

11. Baldwin, B., and Lomax, H.: "Thin Layer Approximation and Algebraic Model for Separated Turbulent Flow," AIAA 78-257, 1978.

12. Degani, D., Schiff, L.B., and Levy, Y.: "Physical Considerations Governing Computation of Turbulent Flows Over Bodies at Large Incidence," AIAA Paper 90-0096, Jan. 1990.

13. Gloss, B. B.: "Current Status and Some Future Test Directions for the US National Transonic Facility," Wind Tunnels and Wind Tunnel Test Techniques, R. Aeronaut. Soc., 1992, pp. 3.1-3.7.

14. Igoe, W.B.: "Analysis of Fluctuating Static Pressure Measurements in the National Transonic Facility," NASA TP-3475, March 1996.

15. Bobbitt, C.W., Hemsch, M.J., and Everhart, J.L.: "NTF Characterization Status," AIAA Paper 2001-755, January 2001.

16. Fuller, D.E.: "Guide for Users of the National Transonic Facility," NASA TM-83124, 1981.

17. Owens, L.R., and Wahls, R.A.: "Reynolds Number Effects on a Supersonic Transport at Subsonic, High-Lift Conditions," AIAA Paper 2001-0911, January 2001.

18. Wahls, R.A., Owens, L.R., and Rivers, S.M.B.: "Reynolds Number Effects on a Supersonic Transport at Transonic Conditions," AIAA Paper 2001-0912, January 2001.

19. Foster, J.M. and Adcock, J.B.: "User's Guide for the National Transonic Facility Research Data System," NASA TM-110242, April 1996.

20. Roe, P.: "Approximate Riemann Solvers, Parameter Vectors, and Difference Schemes," Journal of Computational Physics, Vol. 43, pp. 357-372, 1981.

21. Rivers, M.B., and Wahls, R.A.: "Turbulence Model Comparisons for a High-Speed Aircraft," NASA TP-1999-209540, December 1999.

American Institute of Aeronautics and Astronautics